NOTICE: This is the authors' version of an article that was published in *Fire Safety Journal.* A definitive version is available at https://doi.org/10.1016/j.firesaf.2017.10.003.

Thermal performance of composite slabs with profiled steel decking exposed to fire effects

Jian Jiang, Joseph A. Main, Jonathan M. Weigand and Fahim H. Sadek
National Institute of Standards and Technology (NIST), 100 Bureau Drive, Stop 8611, Gaithersburg, MD, USA, 20899

ABSTRACT

This paper presents a systematic investigation of the influence of various parameters on the thermal performance of composite floor slabs with profiled steel decking exposed to fire effects. The investigation uses a detailed finite-element modeling approach that represents the concrete slab with solid elements and the steel decking with shell elements. After validating the modeling approach against experimental data, a parametric study is conducted to investigate the influence of thermal boundary conditions, thermal properties of concrete, and slab geometry on the temperature distribution within composite slabs. The results show that the fire resistance of composite slabs, according to the thermal insulation criterion, is generally governed by the maximum temperature occurring at the unexposed surface of the slab, rather than the average temperature. The emissivity of steel has a significant influence on the temperature distribution in composite slabs. A new temperature-dependent emissivity is proposed for the steel decking to give a better prediction of temperatures in the slab. The moisture content of the concrete has a significant influence on the temperature distribution, with an increment of 1 % in moisture content leading to an increase in the fire resistance of about 5 minutes. The height of the upper continuous portion of the slab is found to be the key geometrical factor influencing heat transfer through the slab, particularly for the thin portion of the slab. Heat transfer through the thick portion of the slab is also significantly affected by the height of the rib and the width at the top of the rib.

Keywords: composite slab; heat transfer analysis; finite element detailed model; thermal boundary; thermal property; slab geometry

1 Introduction

The use of composite slabs in buildings has been common in North America for many years and has experienced a rapid increase in Europe since the 1980s. Typical construction of composite floors consists of a lightweight concrete slab cast over a profiled steel decking, as illustrated in Fig. 1. The concrete slab typically has welded wire mesh reinforcement to control cracking and may contain individual reinforcing bars, commonly placed within the ribs. Some advantages of composite slabs over conventional flat slabs include requiring less concrete as a result of a low center of reinforcement, and reducing construction time since the decking serves as permanent formwork. The presence of the ribs creates an orthotropic profile, which results in thermal and structural responses that are more complex than those for flat slabs, presenting challenges in numerical analysis and practical design for fire effects.

With regard to the thermal insulation provided by the slab, the temperature at the unexposed top surface is of particular importance, because fire resistance according to the insulation criterion is based on the time required for the unexposed surface temperature to rise by a specified amount (Phan et al. 2010). With regard to the load-bearing capacity of the slab, which governs the fire resistance according to the stability criterion (Phan et al. 2010), the entire through-depth temperature profile of the slab is important, including the temperature of the steel decking and the reinforcement. Reductions in the structural resistance of the slab result from thermally induced degradation in the strength and stiffness of the concrete, the decking, and the reinforcement.

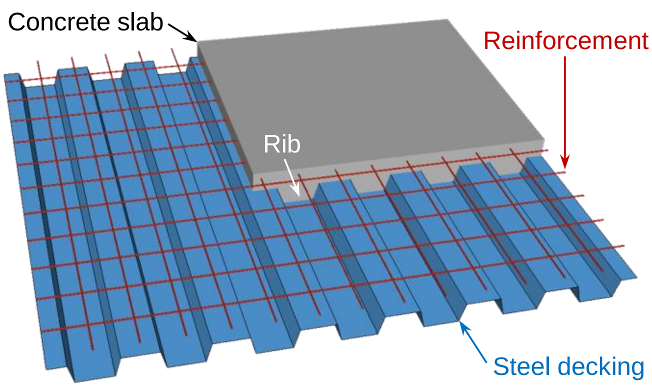

Fig. 1. Typical layout of a composite slab

Challenges in numerical analysis of heat transfer in composite slabs include appropriate modeling of the thermal boundary conditions on the fire-exposed surfaces and proper modeling of heat transfer at the interface between the concrete slab and the steel decking. Previous studies have generally used a detailed finite-element modeling approach, with solid elements for the concrete slab and shell elements for the steel decking. Researchers from the Netherlands Organisation for Applied Scientific Research (TNO) developed 2D and 3D thermal models of fire-exposed composite slabs in which an artificial void was introduced to model the radiation heat exchange between the fire environment and the steel decking (Hamerlinck et al. 1990; Both et al. 1992; Both 1998). The artificial void was bounded by an additional artificial surface where the ISO 834 (International Organization for Standardization, 2014) standard fire curve was specified. This method avoided the introduction of empirical view factors. Lamont et al. (2004) and Guo (2012) introduced interface elements to model heat transfer between the steel deck and the concrete slab in finite-element thermal analyses of composite slabs. Pantousa and Mistakidis (2013) simplified the modeling of this interface in thermo-mechanical analysis of composite slabs by sharing nodes between the shell elements, representing the steel decking, and the solid elements, representing the adjacent concrete, assuming continuity of temperature at their interface.

Most of the previous studies of composite slabs in fire have focused on the structural response, with thermal analysis of the slab being used to provide input for the structural model. Few studies have systematically investigated the temperature distribution in composite slabs and its sensitivity to various parameters. Both (1998) conducted parametric studies by varying the geometry of slabs using 2D thermal models, and the results were used to propose approximate closed-form expressions for the fire resistance based on the thermal insulation criterion, the temperature of reinforcement and decking, and the isotherms in composite slabs. These closed-form approximations are incorporated in Annex D of Eurocode 4 (EN1994-1-2, 2005), hereafter referred to as EC4. However, as is discussed later in this paper, the range of slab geometries considered by Both (1998) does not encompass the dimensions of many composite slabs used in current practice. Lamont et al. (2001) conducted parametric studies to investigate the factors that most influence the temperature distribution in composite slabs. The results showed that the key factors were the conductivity of concrete, the moisture content of concrete, and the convective heat transfer coefficient at the fire-exposed surface. However, no steel decking was considered in the thermal model, and thus some key effects of the decking were not considered, including the temperature-dependent emissivity of the galvanized steel decking that results from melting of a zinc coating, as discussed later in this paper.

The focus of this study is to validate a detailed finite-element modeling approach for heat transfer analysis of composite slabs against experimental measurements available in the literature, and to conduct a parametric study using the validated model to systematically investigate the influence of various parameters on the thermal performance of composite slabs. The parametric study presented herein considers a broader range of parameters than those used by Both (1998), to encompass the geometry of composite slabs used in current practice. A key motivation for the detailed modeling presented in this study was the development of a reduced-order modeling approach presented by Jiang et al. (2017), in which alternating strips of layered composite shell elements were used to represent the thick and thin portions of the composite slab. The reduced-order modeling approach allows engineers to efficiently analyze and evaluate large structural systems exposed to fires, thus facilitating the investigation of three-dimensional effects associated with localized and traveling fires. Calibration and verification of the reduced-order modeling approach required a validated detailed modeling approach that was capable of capturing the influence of various thermal and geometric parameters on heat transfer in composite slabs. Following Pantousa and Mistakidis (2013), the detailed modeling approach in this study used solid elements for the concrete slab and shell elements for the steel decking, with shared nodes at their interface. After validating the detailed finite-element modeling approach against experimental data, detailed models were used to conduct a parametric study by varying the thermal boundary conditions, thermal properties of concrete, and geometric parameters of composite slabs to investigate the influence of these parameters on the thermal performance of composite slabs.

2 Heat transfer analysis

2.1 Heat equation and boundary conditions

Heat can be transferred by three methods: conduction, convection, and radiation. Conduction is the transfer and distribution of heat energy from atom to atom within a substance. Convection is the transfer of heat by the movement of medium (i.e., advection and/or diffusion of a gas or liquid). Radiation is the transfer of heat via electromagnetic waves. The heat conduction balance in a solid structural member under fire conditions is given by the heat equation (e.g., Lienhard 2011):

$$\lambda_x \frac{\partial^2 T}{\partial x^2} + \lambda_y \frac{\partial^2 T}{\partial y^2} + \lambda_z \frac{\partial^2 T}{\partial z^2} = \rho c \frac{\partial T}{\partial t} \tag{1}$$

where λ_x, λ_y, and λ_z are the thermal conductivities of the material in the x, y, z, directions, respectively; T is the temperature; t is time; ρ is the density of the material; and c is the specific heat of the material.

To solve Eq. (1), heat transfer boundary conditions (i.e., convection and radiation heat fluxes) should be provided on the surface between the structural member or fireproofing and gas environment. The boundary conditions can be written as:

$$-\lambda_n \frac{\partial T}{\partial n} = \dot{q}_c'' + \dot{q}_r'' = h_c (T_s - T_g) + \sigma \varepsilon_r \Phi (T_s^4 - T_g^4) \tag{2}$$

where n is a coordinate in the direction of the surface normal; $\dot{q}_c''$ is the heat flux per area from convection, W/m^2; $\dot{q}_r''$ is the heat flux per area from radiation, W/m^2; T_g is the temperature of the gas adjacent to the surface, K; T_s is the surface temperature, K; h_c is the convective heat transfer coefficient, W/(m^2·K); ε_r is the resultant emissivity, defined as $\varepsilon_r = \varepsilon_f \times \varepsilon_s$, where ε_f is the emissivity of fire, usually taken as equal to 1.0, and ε_s is the emissivity of the surface material; $\sigma = 5.67\times10^{-8}$ W/(m^2·K^4) is the Stefan-Boltzmann constant; and Φ is the view factor or configuration factor, which is explained in the next section.

2.2 View factor

The view factor Φ in Eq. (2) quantifies the geometric relationship between the surface emitting radiation and the surface receiving radiation. The view factor depends on the areas and orientations of the surfaces, as well as the gap between them. For composite slabs subjected to standard fires or post-flashover conditions, the view factor of the lower flange of steel decking is generally taken as unity, $\Phi_{low} = 1.0$. The view factors for the web and upper flange of steel decking are less than unity due to obstruction from the ribs. The latter can be calculated following the Hottel's crossed-string method (Nag 2008), as illustrated in Fig. 2, which is also the approach adopted by EC4. Resulting expressions for the view factors of the upper flange and the web of the steel decking, denoted Φ_{up} and Φ_{web}, respectively, are presented in Eqs. (3a) and (3b), where the geometric parameters h_1, h_2, l_1, l_2, and l_3 are illustrated in Fig. 2.

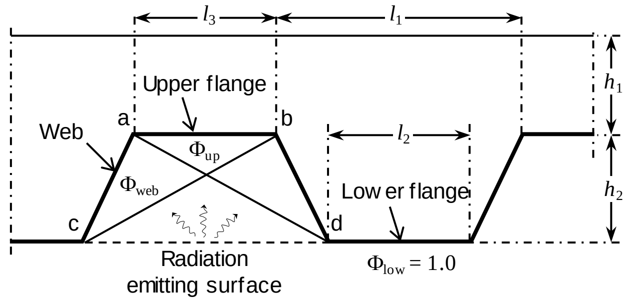

Fig. 2. Schematic for the calculation of view factor

$$\Phi_{\mathrm{up}} = \frac{ad + cb - ab - cd}{2ab} = \frac{\sqrt{h_2^2 + \left(l_3 + \dfrac{l_1 - l_2}{2}\right)^2} - \sqrt{h_2^2 + \left(\dfrac{l_1 - l_2}{2}\right)^2}}{l_3} \tag{3a}$$

$$\Phi_{\mathrm{web}} = \frac{ac + cd - ad}{2ac} = \frac{\sqrt{h_2^2 + \left(\dfrac{l_1 - l_2}{2}\right)^2} + \left(l_3 + l_1 - l_2\right) - \sqrt{h_2^2 + \left(l_3 + \dfrac{l_1 - l_2}{2}\right)^2}}{2\sqrt{h_2^2 + \left(\dfrac{l_1 - l_2}{2}\right)^2}} \tag{3b}$$

2.3 Detailed finite-element modeling

In the detailed finite-element modeling approach, the concrete slab was modeled with solid elements and the steel decking was modeled with shell elements. The concrete slab and steel decking had a consistent mesh at their interface and shared common nodes. Noting the periodicity of the composite slab profile and the thermal loading, with the gas temperature T_g assumed to be uniform, only one half-strip of the composite slab was modeled, as shown in Fig. 3. Adiabatic boundary conditions were assigned at the right and left boundaries of the model to represent the symmetry at these sections in the periodic slab profile. Convection and radiation boundary conditions were defined at the top surface of the slab and the bottom surface of the steel decking (i.e., the lower flange, web, and upper flange of the decking labeled in Fig. 3). Although three-dimensional analyses were performed, with multiple rows of solid and shell elements in the longitudinal direction (i.e., in the direction of the ribs), only two-dimensional heat transfer problems were considered in this study, with the thermal loading and the resulting temperatures assumed uniform in the longitudinal direction. The heat transfer analyses were performed using the LS-DYNA finite-element software (LSTC, 2014). Steel reinforcement was not explicitly included in the numerical models, but reinforcement temperatures, when needed, can be estimated from the temperature of the concrete at the reinforcement location. Both the concrete and the steel decking were modeled using LS-DYNA thermal material model MAT_T10 (MAT_THERMAL_ISOTROPIC_TD_LC), with the specific heat and thermal conductivity for each material defined as functions of temperature using equations from EC4.

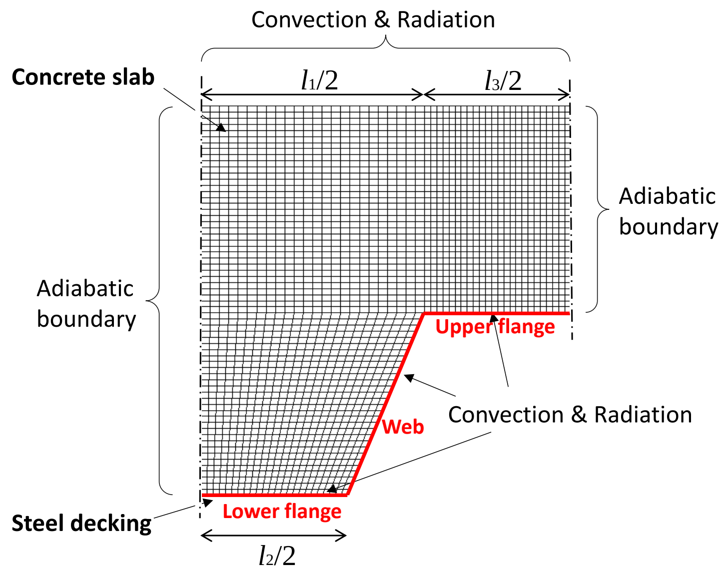

Fig. 3. Schematic of the detailed model of composite slabs

3 Validation of detailed modeling approach

3.1 TNO Test

A standard fire test per ISO 834 (International Organization for Standardization, 2014) on a simply supported one-way concrete slab (Test 2 from Hamerlinck et al. 1990) was selected to validate the proposed detailed modeling approach. Fig. 4 shows the configuration of the tested slab. The slab had six ribs and used Prins PSV73 steel decking and normal-weight concrete with a measured moisture content of 3.4 %. Heat transfer parameters reported by Hamerlinck et al. (1990) were used in the modeling, as summarized in the following. The convective heat transfer coefficient for the lower flange of the steel decking was 25 W/(m^2·K), and a lower value of 15 W/(m^2·K) was used for the web and upper flange of the decking to consider the shielding effect of ribs. A convective heat transfer coefficient of 8 W/(m^2·K) and an emissivity of 0.78 were used for the unexposed top surface of the concrete. View factors for the upper flange and the web of the steel decking were calculated from Eqs. (3a,b) as 0.3 and 0.6, respectively, and a view factor of 1.0 was used for the lower flange of the steel decking and the unexposed top surface of the concrete. The steel decking of composite slabs is usually made from galvanized cold-formed steel with a thin zinc layer on both faces for protection against corrosion. During heating, the zinc layer melts and deteriorates, leading to a delay in the temperature increase of the decking. This effect can be considered in thermal analysis by using a temperature-dependent emissivity of steel. Hamerlinck et al. (1990) proposed using an emissivity of 0.1 for temperatures below 400 °C, and 0.4 for temperatures in excess of 800 °C, with a linear variation in emissivity between 400 °C and 800 °C. For the emissivity of the galvanized steel decking, in addition to the temperature-dependent model of Hamerlinck et al. (1990), two alternative models were considered: the constant value of 0.7 used in EC4 and a new model proposed in this study, which is described subsequently.

Calculated and measured temperature histories are compared in Fig. 5 for several locations in the slab (letters A through K correspond to the temperature measurement points shown in Fig. 4). The numerical results in Fig. 5 used the model of Hamerlinck et al. (1990) for the emissivity of the decking. The largest percent discrepancy between the measured and computed temperatures at the end of the test was about 10 % (at points A and B). The percent deviation at the end of the test is used throughout this paper to quantify discrepancies between computed and measured temperatures for two reasons. Firstly, deviations are of greatest concern for the maximum temperatures in the latter stages of heating, which are the most critical in design. Secondly, percent deviations are not very meaningful in the early stages of heating when the temperatures (in °C) have small numerical values. For the results in Fig. 5, the agreement between the computed and measured temperatures was generally better in the upper continuous part of the slab (points E through K) than in the rib (points A through C). This is most likely because the temperatures in the rib are strongly dependent on the geometry of the steel decking where the isotherms are very steep (shown later in Fig. 9), while the isotherms in the upper portion of the slab are significantly flatter. This behavior was more noticeable in this slab because of the unusually small width of the upper flange of 20 mm.

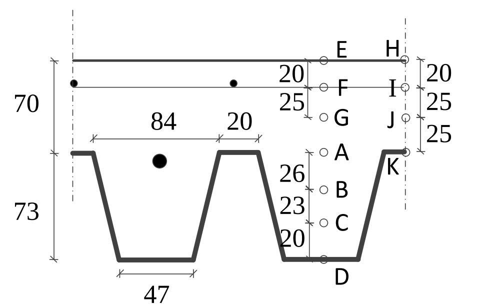

Fig. 4. Geometry of TNO tested slab (Hamerlinck et al. 1990) (dimensions in mm)

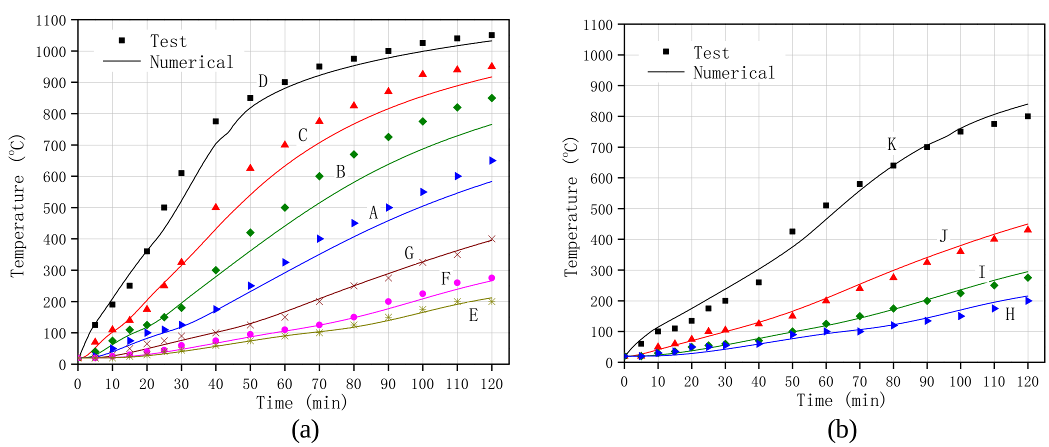

Fig. 5. Comparison of calculated (solid curves) and measured (discrete symbols) temperatures at: (a) the thick part; (b) the thin part

The difference between the numerical and test results in Fig. 5 (especially at Points A, B, and C) was likely due to the influence of the change in emissivity of the galvanized steel decking as a result of melting of the zinc layer, since the predicted temperatures were somewhat lower than the measured results, and since the difference was more pronounced after 30 minutes of heating, when the temperature of the decking exceeded 400 °C. The EC4 conservatively recommends a temperature-independent emissivity value of 0.7 for steel. Fig. 6 shows a comparison of the temperature histories at Points A, B, and C between the test results, the detailed model results based on the constant EC4 emissivity, and the detailed model results based on the temperature-dependent emissivity from Hamerlinck et al. (1990). It shows that the predicted temperatures based on the Hamerlinck model were closer to the test results in the early stage of heating (up to 30 min), while the EC4 predictions were closer to the test results in the later stages of heating (after 80 min). This indicates that the larger emissivity of 0.7 may be more appropriate than 0.4 for temperatures exceeding 800 °C. In this study, a new model for the temperature-dependent emissivity of steel is proposed as follows:

$$\varepsilon_s = \begin{cases} 0.1 & T \leq 400\,°\mathrm{C} \\ 0.1 + 0.0015 \cdot (T - 400\,°\mathrm{C}) & 400\,°\mathrm{C} < T < 800\,°\mathrm{C} \\ 0.7 & T \geq 800\,°\mathrm{C} \end{cases} \tag{4}$$

where at temperatures below 400 °C and above 800 °C, emissivities of 0.1 and 0.7, respectively, are assumed, with a linear variation between 0.1 and 0.7 for temperatures between 400 °C and 800 °C. Fig. 7 shows a comparison of the temperature histories at Points A, B, and C between the test results, detailed model results based on emissivity from Hamerlinck et al. (1990), and detailed model results based on the emissivity model proposed in this study. This figure shows that the increased emissivity at larger temperatures yields higher temperatures by up to 70 °C (Point B at time 90 mins) when compared with the temperature histories using the emissivity from Hamerlinck et al. (1990). Better agreement with the experimental results was observed using the proposed emissivity of steel in Eq. (4). Fig. 8 shows a comparison of temperature histories in the slab between test results and detailed model with the proposed emissivity of steel in Eq. (4). The differences between the measured and computed temperatures at the end of the test in this case did not exceed 5 %. The temperature contours in the slab for the two emissivity models after two hours of heating are shown in Fig. 9. The proposed emissivity of steel decking resulted in high temperatures in a larger area of concrete in the rib.

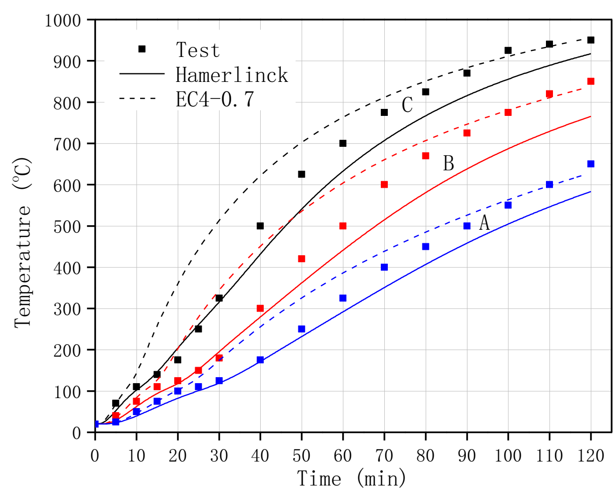

Fig. 6 Comparison of temperature in the rib between test, EC4 and Hamerlinck model

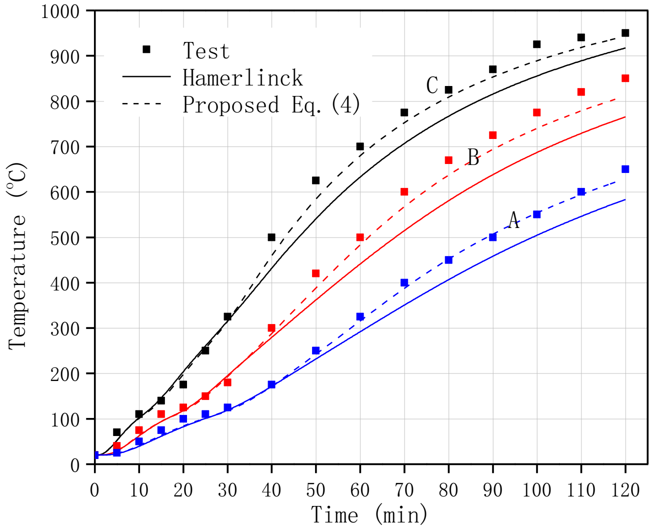

Fig. 7. Comparison of temperature in the rib between test results and numerical model based on emissivity from Hamerlinck et al. (1990) and from proposed model

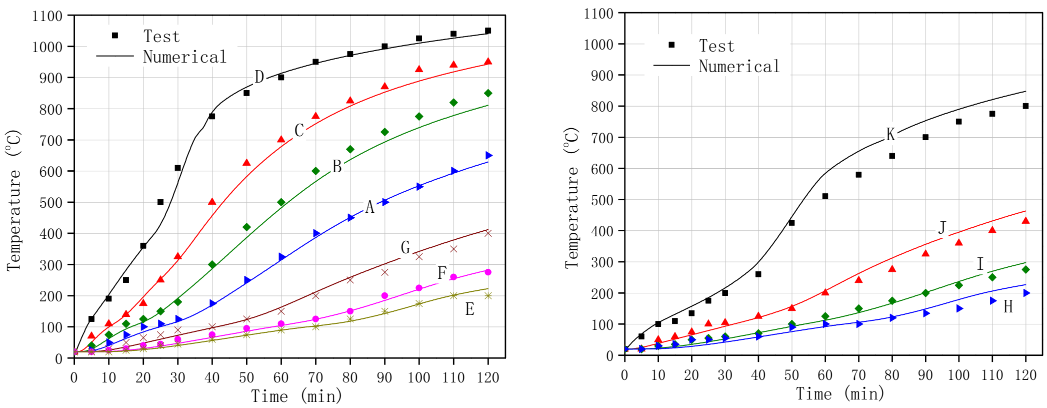

(a) (b)

Fig. 8. Comparison of measured (discrete symbols) and calculated (solid curves) temperatures using proposed emissivity of decking in Eq. (4) at: (a) the thick part; (b) the thin part

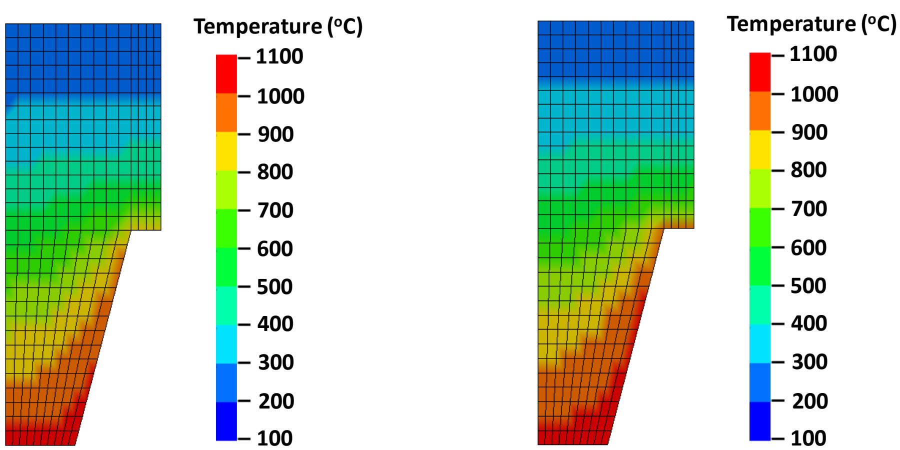

(a) (b)

Fig. 9. Temperature contours in the tested slab (at 120 min): (a) emissivity from Hamerlinck et al. (1990); (b) proposed emissivity in Eq. (4)

3.2 Building Research Association of New Zealand (BRANZ) Test

The detailed modeling approach was also validated against a two-way composite slab tested in the BRANZ furnace (Lim, 2003). The configuration of the slab's cross section is shown in Fig. 10. The tested slab was 3.15 m wide and 4.15 m long, and was exposed to the ISO 834 fire for 3 hours. The Dimond Hibond steel decking had a thickness of 0.75 mm and the total slab depth was 130 mm. Normal-weight concrete was used with siliceous aggregates. In the detailed model of the slab, the same thermal loading and boundary conditions as the TNO test were used. Heat transfer analyses were conducted using steel emissivity from Hamerlinck et al. (1990) and from the model proposed in this study (Eq. (4)). Comparison of numerical and experimental results is presented in Fig. 11 for Points A through E (shown in Figure 10).

Fig. 11 shows only small differences between the temperatures predicted by the two emissivity models. The largest percent deviation between the experimental and computational results at the end of the test was 12 % for the emissivity model of Hamerlinck et al. (1990) and 10 % for the proposed emissivity model, both at point D. The largest-magnitude deviation between the test and model results was observed at point A, which was located at the bottom surface of the concrete slab, where maximum temperature deviations of 135 °C and 192 °C were observed for the model of Hamerlinck et al. (1990) and for the proposed emissivity model, respectively, with corresponding percent deviations of 9 % and 10 % at the end of the test. The large temperature differences at point A were due to debonding of the steel decking from the concrete slab that was observed in the test (Lim, 2003), which disrupted the heat transfer from the steel decking to the lowermost surface of the concrete slab in the experiment, leading to lower measured temperatures. Numerical results provided by Lim (2003) are also included in Fig. 12 for comparison.

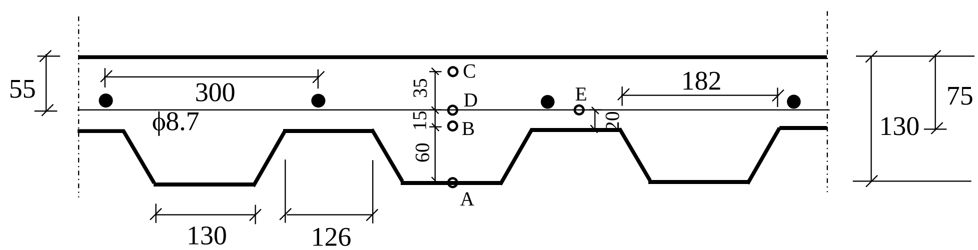

Fig. 10. Geometry of BRANZ tested slab (Lim 2003) (dimensions in mm)

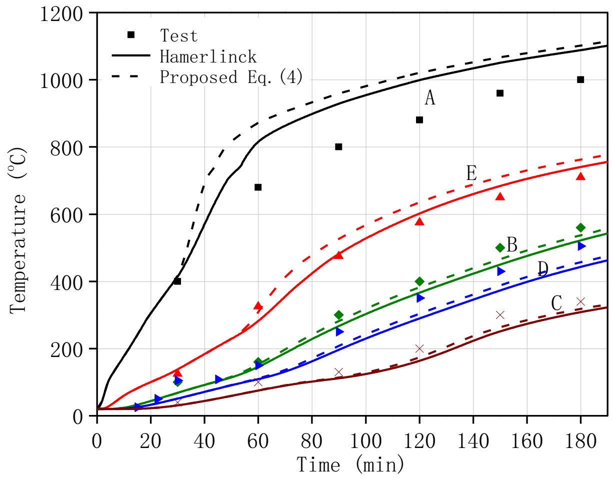

Fig. 11. Comparison of measured temperatures (discrete symbols) with computed temperatures using different emissivity models

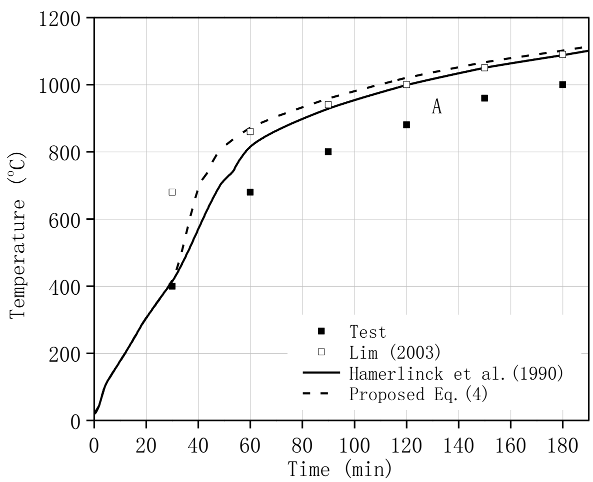

Fig. 12. Comparison of measured and computed temperatures at Point A

4 Parametric study

The detailed modeling approach was used to perform a parametric study on the thermal behavior of composite slabs. The fine mesh shown in Fig. 3 was used throughout this section. The typical composite slab configuration illustrated in Fig. 13, with Vulcraft 3VLI decking, with a thickness of 0.9 mm, was selected as the baseline configuration for this parametric study. Lightweight concrete was used for the baseline configuration due to its common usage in practice. The ISO 834 standard fire curve was used to determine the gas temperature at the fire-exposed surface of the slabs. The following baseline modeling parameters were adopted in the numerical analyses: (1) the convective heat transfer coefficient was taken as 25 W/(m^2·K) for the lower flange and 15 W/(m^2·K) for the web and the upper flange, to consider the shielding effect of the ribs; a value of 8 W/(m^2·K) was taken for the unexposed surface of the slab; (2) a temperature-dependent emissivity of steel based on Hamerlinck et al. (1990) was used (0.1 for T < 400 °C and 0.4 for T > 800 °C); (3) the view factor for the upper flange and web was calculated based on Eq. (3); (4) The moisture content was taken as 5 % for lightweight concrete, which determined the specific heat; and (5) the thermal properties of the concrete were adopted from the EC4 using the upper limit for the thermal conductivity, as explained later in this paper (Fig. 21) and in Jiang et al. (2017).

A survey was conducted on composite slab geometries considered in recent experimental and numerical studies. The results of the survey, shown in Table 1, was the basis for the range of geometric parameters used in the parametric study in this paper. Table 2 shows the range of all parameters considered for the parametric study. Note that the lower and upper bounds of the geometrical parameters h_1, h_2, l_1, l_2, and l_3 in Table 2 are different from the range of applicability of slab geometries in EC4, which uses the ranges of $h_1 = 50$ mm to 125 mm, $h_2 = 50$ mm to 100 mm, $l_1 = 80$ mm to 155 mm, $l_2 = 32$ mm to 132 mm, and $l_3 = 40$ mm to 115 mm. For the parametric study, baseline values were used in a given analysis and only one parameter was changed at a time.

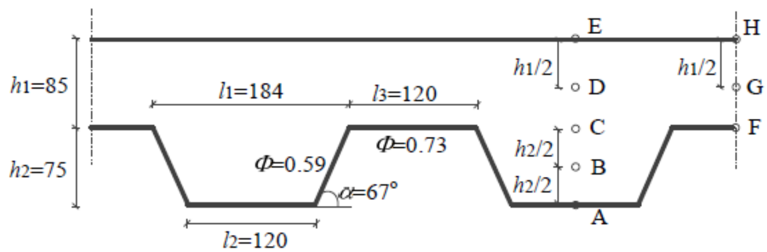

Fig. 13. Configuration of Vulcraft 3VLI

Table 1. Summary of composite slab properties from previous studies (see Fig. 13)

Reference	Type of Decking	Slab Dimensions (mm)					Φ_{up}
		h_1	h_2	l_1	l_2	l_3	
TNO Tests (Hamerlinck et al. 1990)	Prins PSV 73	70	73	84	47	20	0.36
	PMF CF 60	70	60	169	120	131	0.78
	Cofrastra 70	75	70	113	87	70	0.53
	Ribdeck 60	60	90	185	155	115	0.58
Cardington tests (Kirby 1997)	PMF CF70	70	60	188	136	112	0.76
Bailey et al. (2000)	PMF F60	90	60	136	90	64	0.65
Tongji Tests (Li and Wang 2013)	-	70	76	202	142	142	0.75
BRANZ (Lim et al. 2004)	Hibond	75	55	182	130	126	0.80
Wellman et al. (2011)	Vulcraft 1.5VLR	64	38	108	88	44	0.61
Guo and Bailey (2011)	PMF CF60	85	60	169	120	131	0.78
COSSFIRE (Zhao et al. 2011)	COFRAPLUS 60	97	58	101	62	107	0.73
Main and Sadek (2012)	Vulcraft 3VLRI	83	76	172	132	132	0.69
Bednar et al. (2013)	TR40/160	40	38	110	50	50	0.80
Pantousa and Mistakidis (2013)	-	77	73	96	50	92	0.65

Table 2. Ranges for parameters used in the parametric study

Parameter	Baseline	Lower Bound	Upper Bound
Thermal Boundary Conditions			
Convective heat transfer coefficient for fire-exposed decking, $h_{c,deck}$	Lower flange: 25 W/(m^2·K) Web, upper flange: 15 W/(m^2·K)	15 W/(m^2·K)	35 W/(m^2·K)
Convective heat transfer coefficient for unexposed top surface, $h_{c,top}$	8 W/(m^2·K)	4 W/(m^2·K)	9 W/(m^2·K)
Emissivity of decking, $\varepsilon_{s,deck}$	T < 400 °C: 0.1 T > 800 °C: 0.4	0.1	0.7
Emissivity of concrete, $\varepsilon_{s,top}$	0.7	0.6	0.8
View factor of web, Φ_{web}	0.59	0.2	0.8
View factor of upper flange, Φ_{up}	0.73	0.2	0.8
Thermal Properties of Concrete			
Type of concrete	Lightweight	Lightweight	Normal weight
Model for thermal conductivity	EC4 upper limit	EC4 lower limit	EC4 upper limit
Moisture content	5 %	0 %	7 %
Slab Geometry			
Height of concrete topping, h_1	85 mm	50 mm	125 mm
Height of rib, h_2	75 mm	50 mm	100 mm
Width at top of rib, l_1	184 mm	130 mm	250 mm
Width of lower flange, l_2	120 mm	80 mm	160 mm
Width of upper flange, l_3	120 mm	80 mm	160 mm

4.1 Influence of thermal boundary conditions

As shown in Eq. (2), the convection and radiation boundary conditions are represented by the convective heat transfer coefficient h_c, the emissivity of the surface material ε_s (galvanized steel on the fire-exposed side and concrete on the unexposed side), and the view factor Φ. In this section, the sensitivity of temperature rise at various locations in composite slabs to these three parameters is examined. The influence of heat input through different surfaces of the steel decking (lower flange, upper flange, and web) is also investigated.

Influence of convective heat transfer coefficient

For the convective heat transfer coefficient of the fire-exposed surface of composite slabs, the EC4 recommends a value of 25 W/(m^2·K) for a standard fire and 35 W/(m^2·K) for a natural fire. Hamerlinck et al. (1990) suggested a smaller coefficient of 15 W/(m^2·K) for the web and upper flange of the decking to consider the reduced rate of heat flux in the void between two consecutive webs. Fig. 14 shows the variation of temperatures in the thick and thin portions of slabs for convective heat transfer coefficients in the range of 15 W/(m^2·K) to 35 W/(m^2·K). The figure shows that the convective heat transfer coefficient has little effect on the temperature distribution in the slab except for at the steel decking (points A and F) during the early stages of heating. The upper flange of the deck (point F) is more sensitive to the coefficient than the lower flange (point A) due to its smaller view factor. As the convective heat transfer coefficient has a minimal influence on deck temperatures in the later stages of heating, its influence on the fire-exposed side can be considered as negligible. This behavior was expected since the concrete temperatures at the later stages of heating are dominated by radiation considering a dependence on T^4, see Eq. (2). A similar observation was also made by Lamont et al. (2001). However, Lamont et al. (2001) indicated a strong dependence of concrete temperatures on the convective coefficient as a result of not including the steel decking in the analysis, and using a small convective heat transfer coefficient of 5 W/(m^2·K) instead to compensate for the missing steel decking.

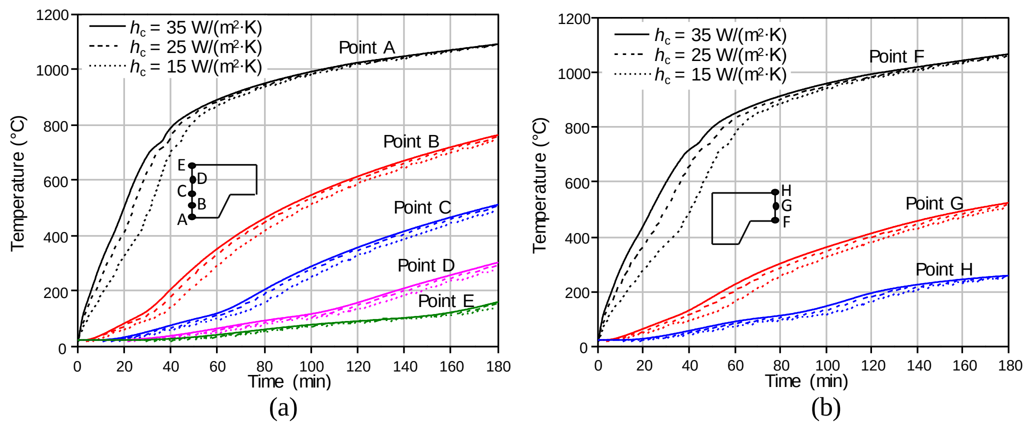

Fig. 14. Temperature histories within composite slabs with varying convective heat transfer coefficient for the fire-exposed surface: (a) thick portion of slab; (b) thin portion of slab.

For the convective heat transfer coefficient for the unexposed top surface of composite slabs, EC4 recommends a value of 4 W/(m^2·K) when heat transfer by radiation is considered, and 9 W/(m^2·K) when heat transfer by radiation is not considered. Hamerlinck et al. (1990) suggested a coefficient of 8 W/(m^2·K) for the unexposed side, while considering radiation effects. Fig. 15 shows the variation of temperatures in the thick and thin portions of the slab for varying coefficients of heat transfer by convection of the unexposed side. The convective heat transfer coefficient was taken as 25 W/(m^2·K) for the lower flange and as 15 W/(m^2·K) for the web and upper flange. In general, the temperature distribution in the slab was not sensitive to the boundary condition at the unexposed surface. Only Point H, located at the unexposed surface of the thin portion of the slab, exhibited a noticeable sensitivity to the thermal boundary condition at the unexposed side.

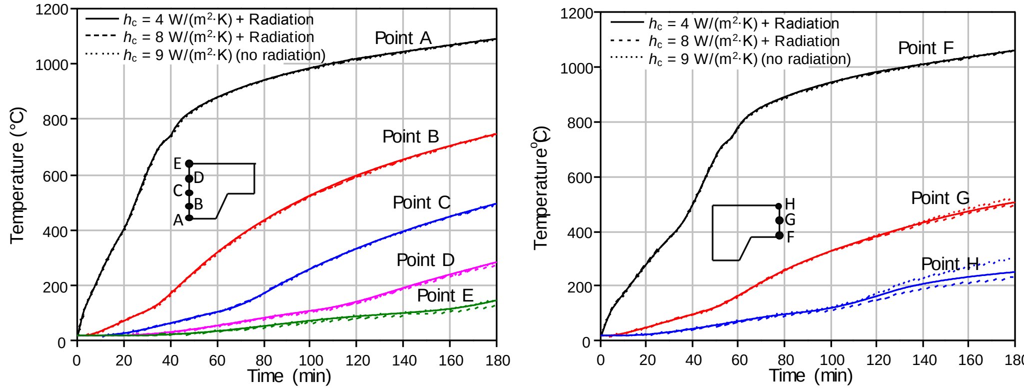

(a) (b)

Fig. 15. Temperature histories within composite slabs with varying convective heat transfer coefficient for the unexposed surface: (a) thick portion of slab; (b) thin portion of slab.

Influence of emissivity

EC4 recommends a value of 0.7 for the emissivity of steel decking of composite slabs. Hamerlinck et al. (1990) suggested a temperature-dependent emissivity of 0.1 for $T \leq 400$ °C and 0.4 for $T \geq 800$ °C to account for melting of the zinc-layer on the decking, and this paper has recommended Eq. (1). To investigate the influence of the emissivity of the steel decking on the temperature distribution in the slab, Fig. 16 shows the variation of temperature distribution in the slab with constant emissivities of 0.1, 0.4, and 0.7 for the steel decking (lower flange, web, and upper flange). When compared to the limited influence of the convective heat transfer coefficient for the fire-exposed side of the slab in Fig. 14, the emissivity of the steel decking had significant influence on the temperature rise in the slab. At a given time, the temperatures at Points A to F decreased with decreasing emissivity. This decrease in temperature is more pronounced for values of emissivity between 0.1 and 0.4 than for values between 0.4 and 0.7. This response was also observed in the study by Lamont et al. (2001), where the emissivity varied between 0.4 and 1.0. It was found that the emissivity had a larger effect on the temperatures near the exposed surface of the slab rather than those near the unexposed surface.

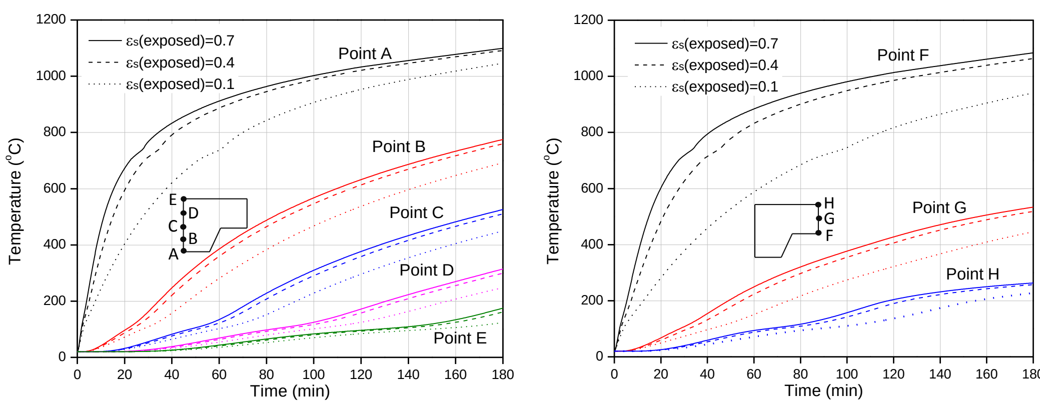

(a) (b)

Fig. 16. Temperature histories within composite slabs with different temperature-independent values for the emissivity of galvanized steel: (a) thick portion of slab; (b) thin portion of slab

Fig. 17 shows a comparison of temperature distribution in the slab between the constant value of 0.7 (based on EC4), the temperature-dependent emissivity of steel decking based on

Hamerlinck et al. (1990), and the proposed emissivity in Eq. (4). The temperature-dependent emissivities resulted in lower temperatures during the early stages of heating, especially for the steel decking (Points A and F). In general, the two temperature-dependent models of emissivity produced similar temperature histories, except at the steel decking (Points A and F). The proposed model for emissivity in Eq. (4) predicted higher temperatures in the steel decking than those produced by the Hamerlinck et al. (1990) model.

The emissivity of concrete at the unexposed top surface of slabs is recommended as 0.7 in EC4 and 0.8 in EN 1991-1-2 (2009). Hamerlinck et al. (1990) suggested a value of 0.78. Fig. 18 shows that the practical range of concrete emissivity of 0.6 to 0.8 had a negligible influence on the temperature rise in composite slabs. Figs. 15 and 18 together show that the thermal boundary conditions on the unexposed side had little to no influence on the temperature distribution in composite slabs.

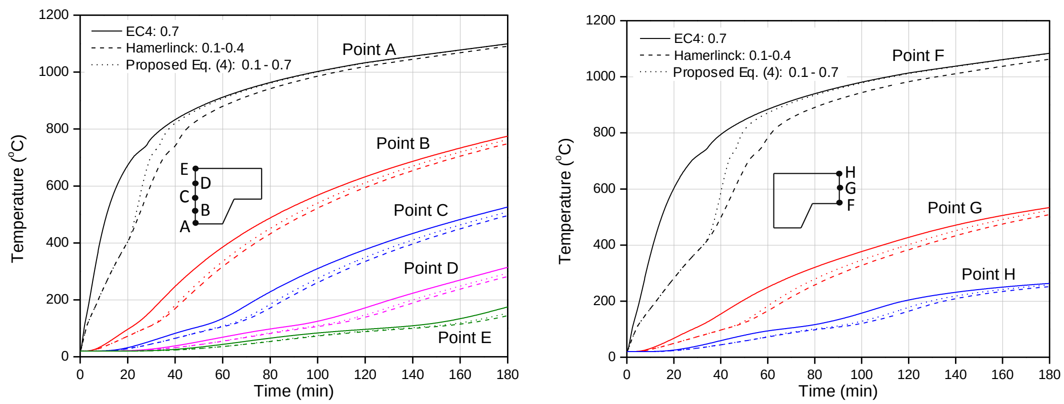

(a) (b)

Fig. 17. Temperature histories within composite slabs with different temperature-dependent models for the emissivity of galvanized steel: (a) thick portion of slab; (b) thin portion of slab

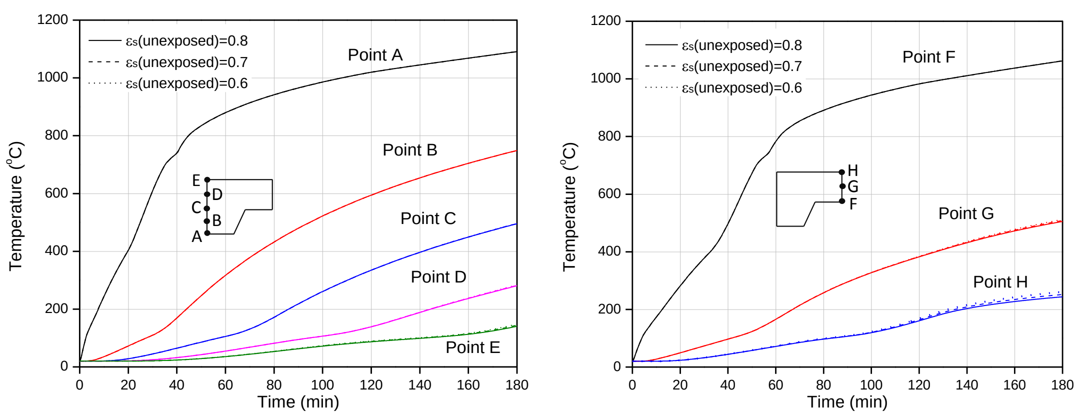

(a) (b)

Fig. 18. Temperature histories within composite slabs with varying constant emissivity of concrete at unexposed side: (a) thick portion of slab; (b) thin portion of slab

Influence of view factor

Fig. 19 shows the variation of temperatures in composite slabs with view factors of the web, Φ_{web}, having values of 0.2, 0.4, and 0.8. For these analyses, the view factor of the upper flange was calculated from Eq. (3a) as Φ_{up} = 0.73. The view factor, Φ_{web}, significantly affected the temperature of the web (Point I) but had a negligible effect on the temperatures in the concrete. Fig. 20 shows the results for varying the view factor of the upper flange, Φ_{up}, with values of 0.2, 0.4, 0.8. For these analyses, the view factor of the web was calculated from Eq. (3b) as Φ_{web} = 0.59. Similar to the previous observations for the emissivity of steel, the temperatures in the thin portion of the slab were sensitive to the view factor of the upper flange, Φ_{up}, while the temperatures in the thick portions were not.

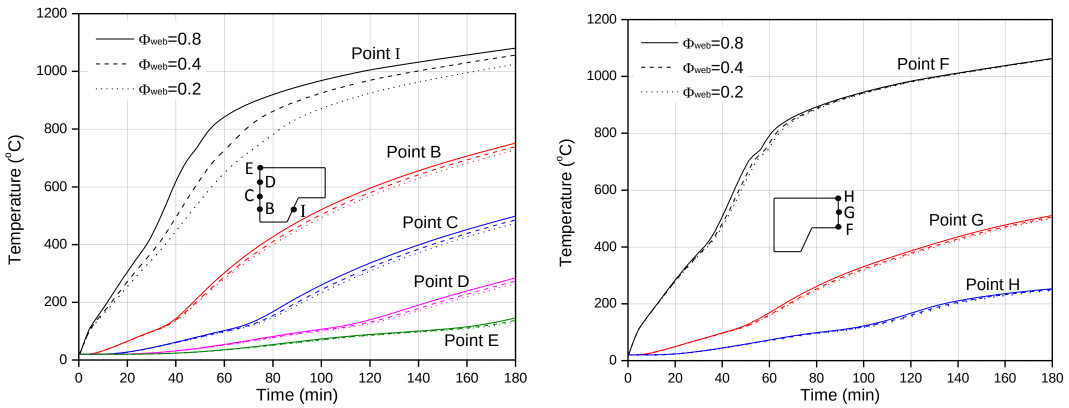

(a) (b)

Fig. 19. Temperature histories within composite slabs with varying Φ_{web}: (a) thick portion of slab; (b) thin portion of slab

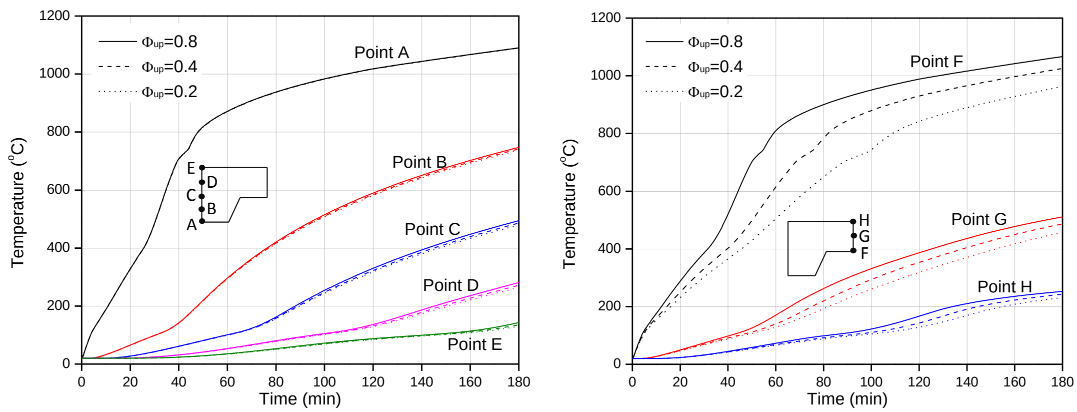

(a) (b)

Fig. 20. Temperature histories within composite slabs with varying Φ_{up}: (a) thick portion of slab; (b) thin portion of slab

4.2 Influence of thermal properties of concrete

The temperature rise in composite slabs depends on the thermal properties of concrete, including density, thermal conductivity, and specific heat. The density of concrete is considered independent of temperature and is taken as 2300 kg/m^3 for normal-weight concrete and 1900 kg/m^3 for lightweight concrete in EC4. The thermal conductivity and specific heat vary with moisture content and aggregate type. Temperature-dependent expressions for these two properties are given in EC4 and in the American Society of Civil Engineers (ASCE) manual on structural fire protection (ASCE 1992), as shown in Fig. 21 and Fig. 22. The ASCE manual distinguishes between siliceous and carbonate aggregates, while EC4 applies to all aggregate types. The influences of the thermal conductivity and specific heat on the temperature distribution in composite slabs are presented in the following sections.

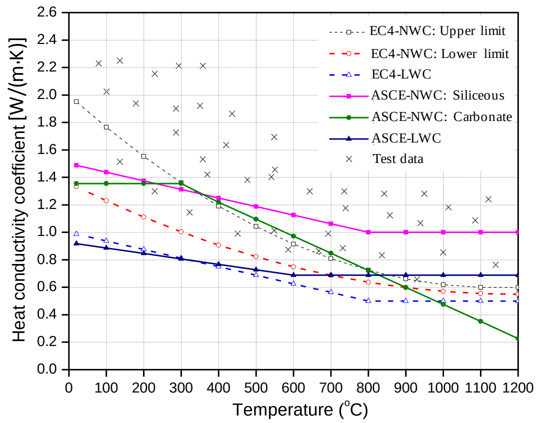

Fig. 21. Thermal conductivity of concrete in EC4 and ASCE along with test data from Kodur (2014)

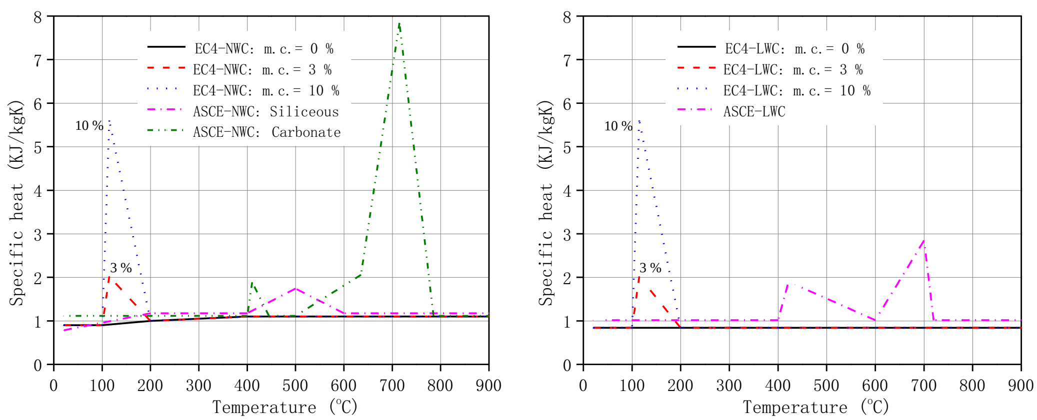

(a) (b)

Fig. 22. Specific heat of concrete in EC4 and ASCE: (a) normal-weight concrete; (b) lightweight concrete

Influence of thermal conductivity

There are significant differences in the temperature-dependent models for the thermal conductivity of concrete (λ) given in EC4 and in the ASCE manual, as shown in Fig. 21. The data from Kodur (2014) are generally higher than the upper-limit model in EC4. To envelope the data, a new upper bound is proposed in this study by assuming linear variation in the conductivity from 2.5 W/(m·K) at 20 °C to 1.25 W/(m·K) at 800 °C, with a constant conductivity of 1.25 W/(m·K) above 800 °C. A set of analyses was performed using the various models for the thermal conductivity of concrete given in EC4 and in the ASCE manual, as well as the newly proposed upper bound.

Fig. 23 shows a comparison of temperature histories in the slab obtained using the various models for thermal conductivity of normal-weight concrete. As expected, the predicted temperatures of concrete increased as the conductivity increased. This is similar to the findings of Lamont et al. (2001). The thermal conductivity of concrete had a larger effect on the temperatures at the unexposed side (points E and H) than on the temperatures at the fire-exposed side (points A and F). Predictions based on the upper-limit model in EC4 typically fell between the predictions based on the lower-limit model in EC4 and the proposed upper bound. Predictions based on the two ASCE models were similar to each other and also to predictions based on the upper-limit model in EC4.

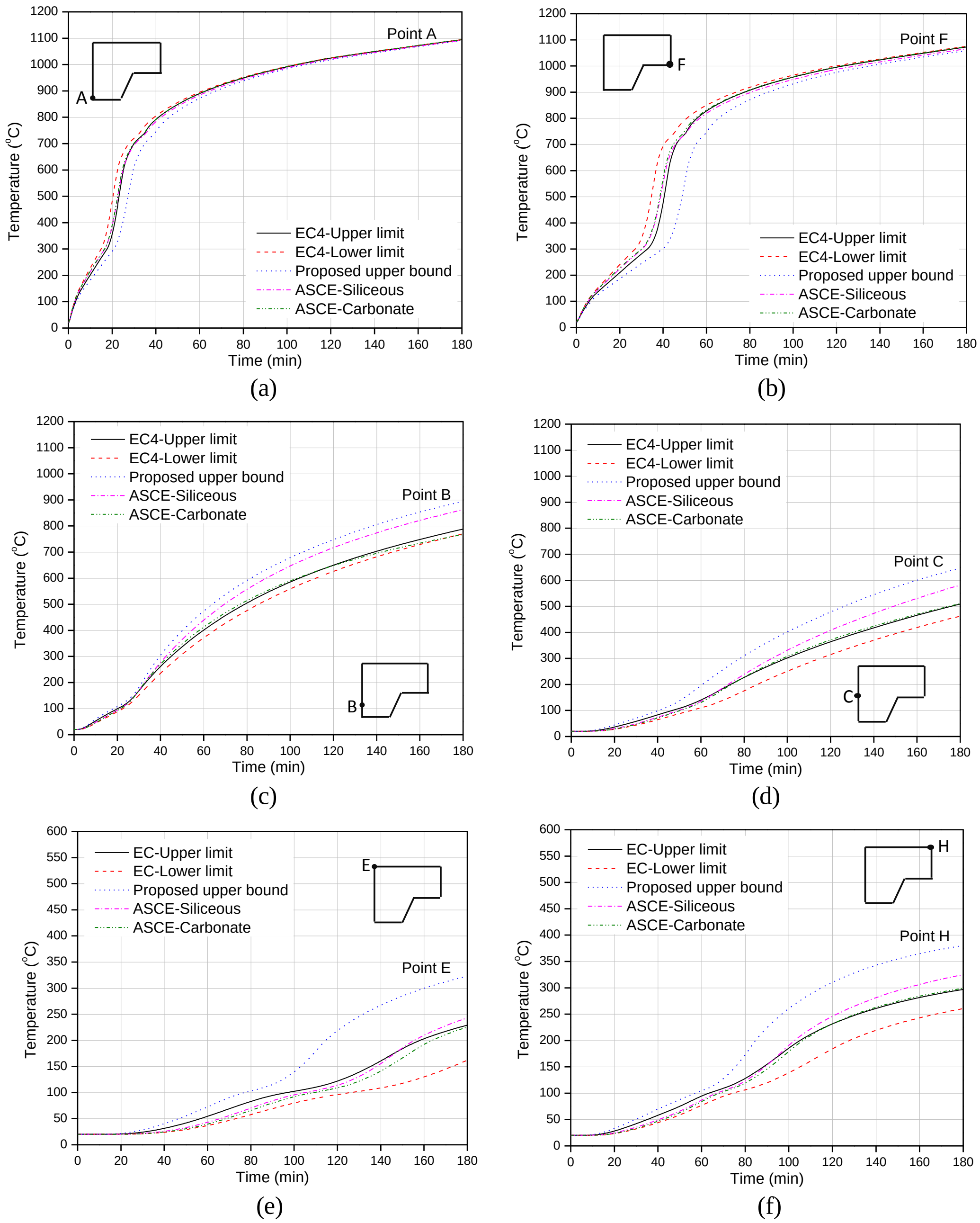

Fig. 23. Temperature histories within composite slabs with different models for concrete conductivity: (a) Point A; (b) Point F; (c) Point B; (d) Point C; (e) Point E; (f) Point H

Influence of specific heat

Fig. 22 shows the specific heat of concrete as a function of temperature for normal-weight and lightweight concrete. The EC4 models for normal-weight and lightweight concrete depend on the moisture content (m.c.). As shown in Fig. 22, the specific heat ranges between approximately 900 J/(kg·K) and 1200 J/(kg·K) for normal-weight concrete and between approximately 840 J/(kg·K) and 1000 J/(kg·K) for lightweight concrete, except at high temperatures between 400 °C and 800 °C in the ASCE manual (due to the phase change of aggregate), and between 100 °C and 200 °C in EC4 (due to the influence of moisture evaporation in the early stage of heating). The exception in the ASCE manual is less significant, since the concrete temperature in a slab does not usually reach 700 °C.

For dry (zero moisture content) normal-weight concrete, constant values of 1000 J/(kg·K) and 1170 J/(kg·K) are recommended for simple calculations in EC4 and in the ASCE manual, respectively. A constant specific heat of 840 J/(kg·K) is recommended for lightweight concrete in EC4. EC4 also recommends a temperature-dependent model for specific heat of dry normal-weight concrete, whereby the specific heat varies between 900 J/(kg·K) and 1100 J/(kg·K). Fig. 24 shows the variation of temperature in the slab when constant values of 1000 J/(kg·K) and 1170 J/(kg·K) are used, as well as when the temperature-dependent model from EC4 is used. The temperatures within the slab for the constant specific heat of 1000 J/(kg·K) agree well with the temperature-dependent model.

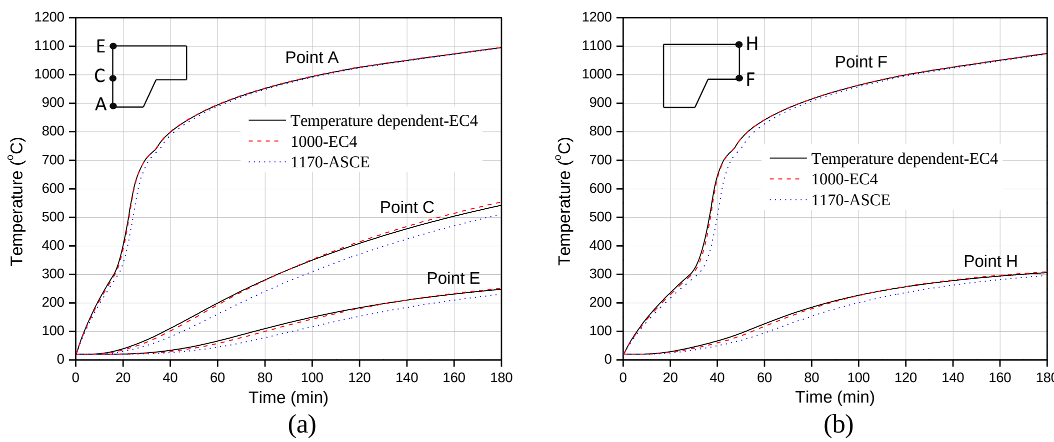

Fig. 24. Temperature histories within composite slabs with varying specific heat (dry normal-weight concrete): (a) thick portion of slab; (b) thin portion of slab

To account for the influence of moisture content (m.c.) of normal-weight concrete on the thermal response of the slabs, the analyses accounted for the spike in the specific heat for temperatures between 100 °C and 200 °C, Fig. 22. The moisture content had a significant influence on the temperatures in the slab, as shown in Fig. 25. As expected, as the moisture content increased, the predicted concrete temperatures decreased. In particular, a delay in the rate of temperature increase was evident at the unexposed surface (Point E) as the temperature passed through 100 °C. This plateau occurring at about 100 °C was also observed in the study by Lamont et al. (2001). This effect was more significant for higher values of moisture content, leading to longer delays in the temperature rise within the concrete, and a plateau in the temperature history at a temperature of 100 °C is clearly evident in Fig. 25(b) for the moisture contents of 5 % and 7 %. After most of the moisture had evaporated (at temperatures exceeding about 150 °C), a more rapid rise in the concrete temperature was observed.

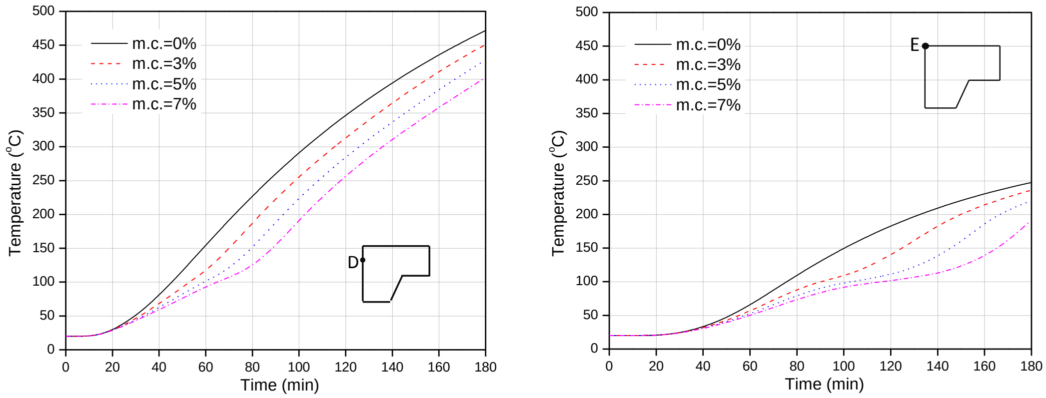

(a) (b)

Fig. 25. Temperature histories within composite slabs with varying moisture content: (a) Point D; (b) Point E

4.3 Influence of slab geometry

The geometry of a composite slab can be represented by the five dimensions illustrated in Fig. 13: h_1, h_2, l_1, l_2, and l_3, which denote, respectively, the height of the upper continuous portion of the slab, the height of the rib, the width at the top of the rib, the width of the lower flange of the decking, and the width of the upper flange of the decking. The influences of these dimensions on the temperature distribution in the composite slab are discussed in the following subsections.

Influence of h_1

Numerical analyses were conducted for three slabs with h_1 = (50 mm, 85 mm, and 125 mm). Temperature contours for the three cases are shown in Fig. 26, while Fig. 27 shows corresponding temperature histories in the thick and thin portions of the slabs. The dimension h_1 had the greatest influence on the temperature of the unexposed surface of the slab, especially in the thin portion (points G and H in Fig. 27(b)). For the largest value of h_1 = 125 mm, plateaus are clearly evident in the temperature histories at points E and H as the temperature passes through 100 °C, due to the effect of increased moisture associated with the larger concrete mass.

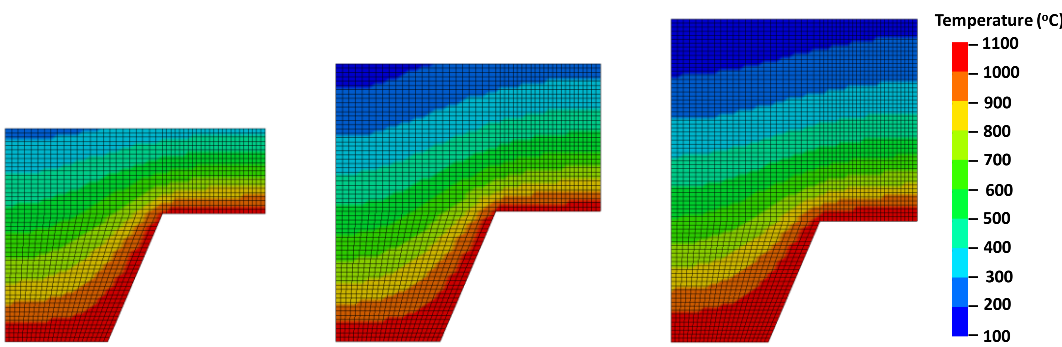

(a) (b) (c)

Fig. 26. Comparison of temperature contours within composite slabs with varying h_1 after 180 min of heating: (a) h_1 = 50 mm; (b) h_1 = 85 mm; (c) h_1 = 125 mm

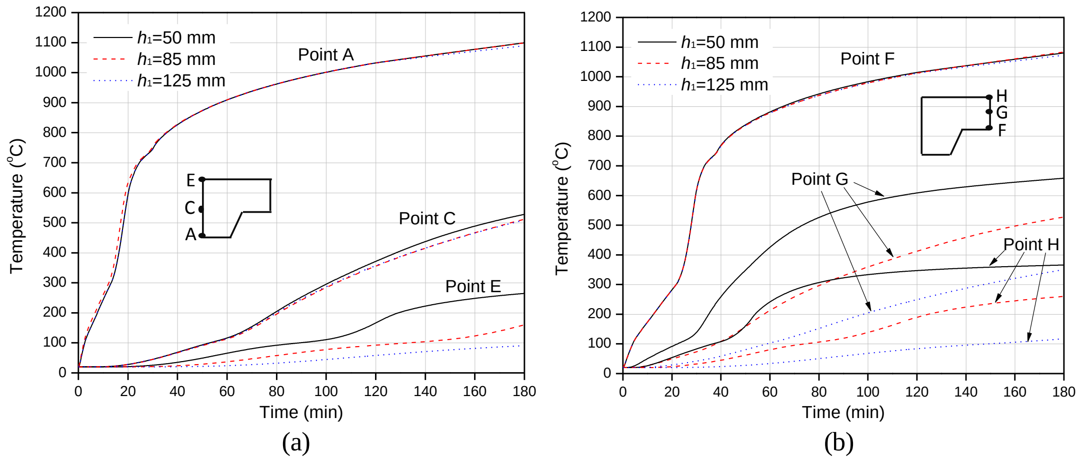

Fig. 27. Temperature histories within composite slabs with varying h_1: (a) thick portion of slab; (b) thin portion of slab

Influence of h_2

Three slabs with different rib heights were modeled (h_2 = 50 mm, 75 mm, and 100 mm), and the results are shown in Figs. 28 and 29. As h_2 was increased, the angle of the web increased, resulting in steeper isotherms, as shown in Fig. 28. Fig. 29 shows that the increased rib height resulted in reduced temperatures at all locations in the slab except for point A. The temperature at point A was virtually unaffected by varying h_2. The reductions in temperature resulted from the increased mass of concrete in the rib, with the most significant reductions in temperature occurring at point C, at the top of the rib.

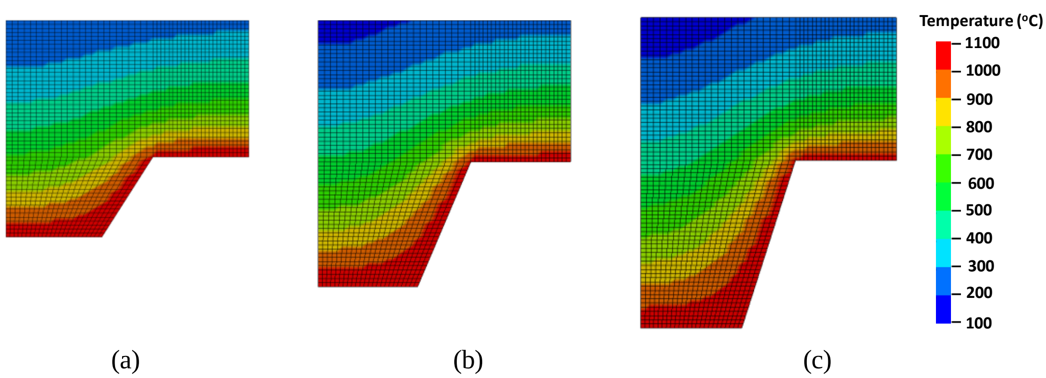

Fig. 28. Comparison of temperature contours within composite slabs with varying h_2 after 180 min of heating: (a) h_2 = 50 mm; (b) h_2 = 75 mm; (c) h_2 = 100 mm

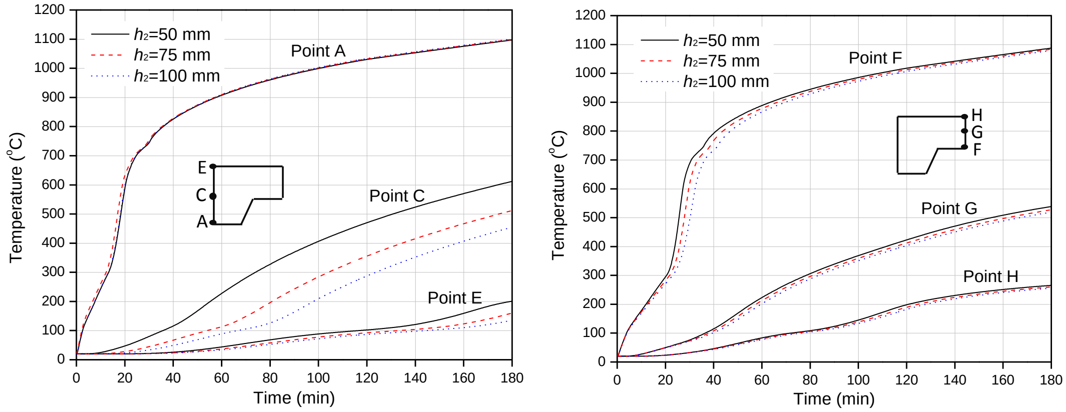

(a) (b)

Fig. 29. Temperature histories within composite slabs with varying h_2: (a) thick portion of slab; (b) thin portion of slab

Influence of l_1

Three slabs with different widths at the top of the rib were modeled (l_1 = 130 mm, 184 mm, and 250 mm), and the resulting temperature contours and temperature histories in the slab are shown in Figs. 30 and 31, respectively. Increasing l_1 increases the mass of concrete in the rib, leading to a reduction of temperatures in the thick part of the slab (points C and E) and a larger region of cooler temperatures above the rib. However, increasing l_1 had a small effect on the temperatures in the thin portion of the slab (points F, G, and H).

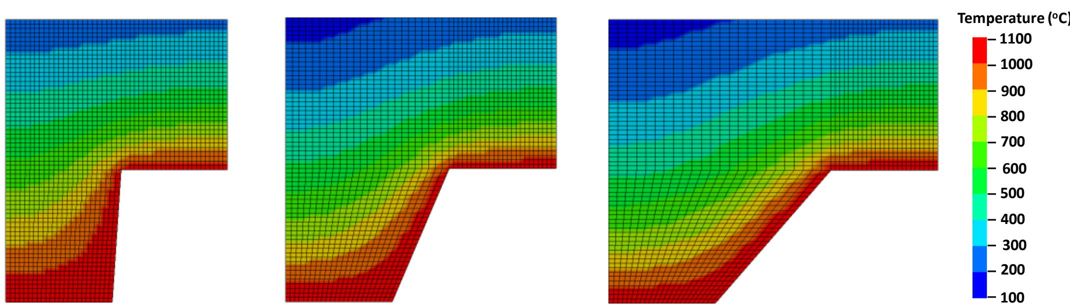

(a) (b) (c)

Fig. 30. Comparison of temperature contours within composite slabs with varying l_1 after 180 min of heating: (a) l_1 = 130 mm; (b) l_1 = 184 mm; (c) l_1 = 250 mm

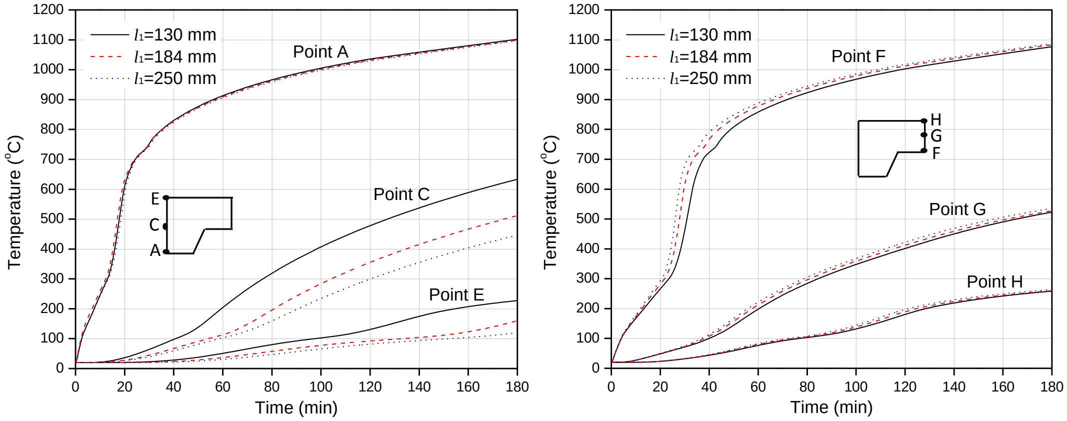

(a) (b)

Fig. 31. Temperature histories within composite slabs with varying l_1: (a) thick portion of slab; (b) thin portion of slab

Influence of l_2

Three slabs with different widths of the lower flange of the decking were modeled (l_2 = 80 mm, 120 mm, and 160 mm), and the resulting temperature contours and temperature histories are shown in Figs. 32 and 33, respectively. Increasing l_2 increases the mass of concrete in the rib, leading to a reduction of temperatures in the thick portion of the slab (at points C and E), although this effect was less significant than for increases in h_2 and l_1. Increasing l_2 had almost no influence on the temperatures in the thin portion of the slab and only slightly affected the temperature contours in the upper continuous portion of the slab, in spite of the significant changes in the angle of the web.

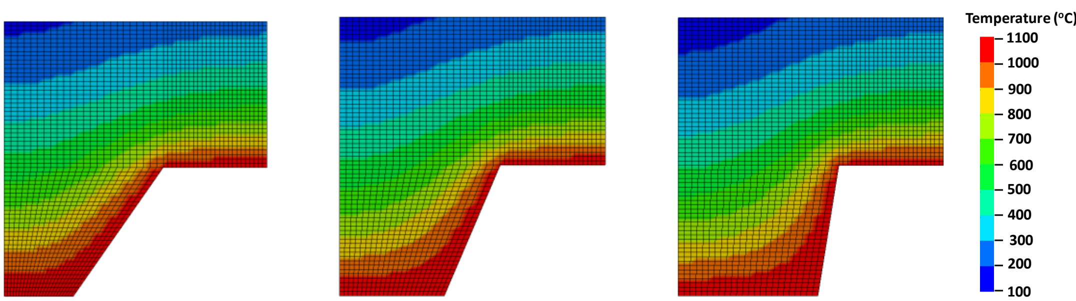

(a) (b) (c)

Fig. 32. Comparison of temperature contours within composite slabs with varying l_2 after 180 min of heating: (a) l_2 = 80 mm; (b) l_2 = 120 mm; (c) l_2 = 160 mm

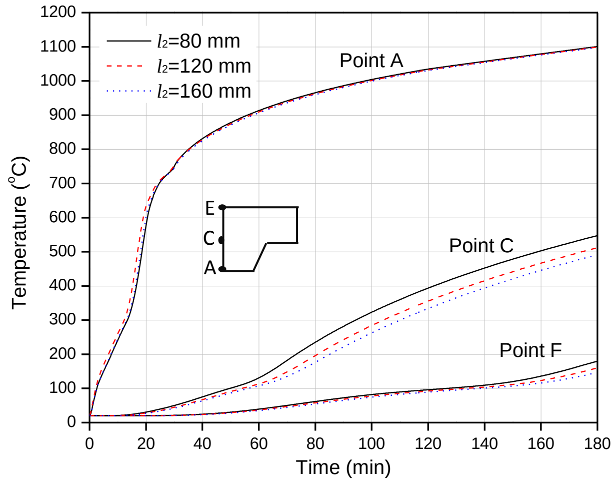

Fig. 33. Temperature histories within composite slabs with varying l_2

Influence of l_3

The width of the upper flange of the decking, l_3, affects the heat transfer through the thin portion of a composite slab, where the maximum temperature occurs at its unexposed side, but has little influence on the shape of the isotherms and the temperature distribution in the thick portion of the slab. Figs. 34 and 35 show, respectively, the computed temperature contours and temperature histories after three hours of heating for three slabs with different upper-flange widths (l_3 = 80 mm, 120 mm, and 160 mm). Although the temperatures in the thin portion of the slab (at points F, G, and H) increased with increasing l_3, this effect was small.

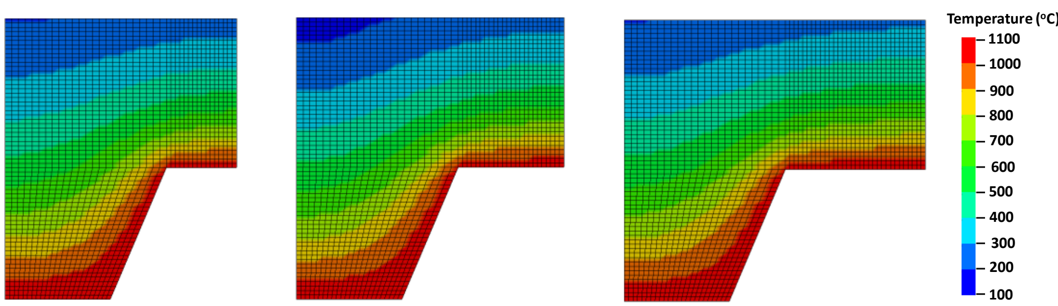

(a) (b) (c)

Fig. 34. Comparison of temperature contours within composite slabs with varying l_3 after 180 min of heating: (a) l_3 = 80 mm; (b) l_3 = 120 mm; (c) l_3 = 160 mm

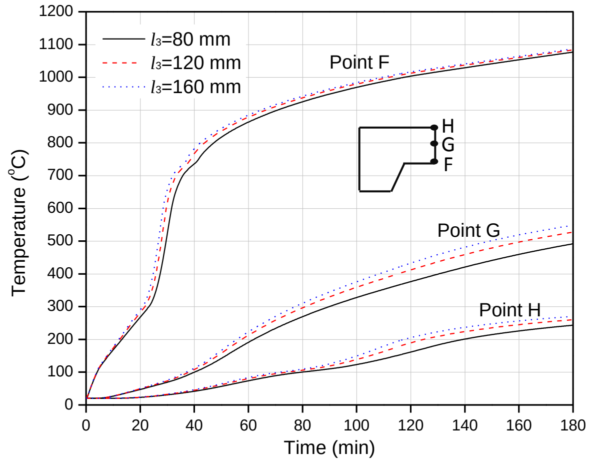

Fig. 35. Temperature histories within composite slabs with varying l_3

5 Fire resistance according to thermal insulation criterion

The temperature rise at the unexposed surface of composite slabs is a major concern from the thermal insulation standpoint. It is important to control the temperature rise to avoid igniting any material on the unexposed surface of the slab, and thus prevent the spread of fire. In EC4, the fire resistance according to the thermal insulation criterion, expressed in minutes, is calculated based on the fire duration until a maximum temperature rise of ΔT = 180 °C or an average temperature rise of ΔT = 140 °C, whichever governs, is reached at the unexposed surface of the slab.

Table 3 shows a comparison of the fire resistance values obtained from numerical analyses described in Section 4 using the various parameters in Table 2. The baseline slab had a fire resistance of 124 min based on the maximum temperature criterion, and 136 min for the average temperature criterion. In general, the maximum temperature criterion, which occurred at the thin portion of the slab, governed the fire resistance of the composite slabs. This indicates that the temperature distribution in the thin portion played a key role in the thermal insulation of composite slabs.

Based on the fire resistance of the baseline configuration and the results presented in Table 3, the factors that most strongly influenced the fire resistance of composite slabs were the thickness of the upper continuous portion of the slab, h_1, the emissivity of the steel decking, $\varepsilon_{s,deck}$, the view factor of the upper flange, Φ_{up}, and the moisture content of concrete. Other parameters had a less significant effect on the fire resistance. In particular, the moisture content had a significant influence on the fire resistance for both normal weight concrete and lightweight concrete slabs. It was found that the fire resistance increased almost linearly with moisture content where an increment of 1 % in moisture content led to an enhancement of the fire resistance by about 5 minutes. Among the slab geometry parameters, the thickness of the upper continuous portion of the slab (h_1) governed the fire resistance. The width of the upper flange (l_3) had an influence since it affected the temperature distribution in the thin portion where the maximum temperature occurred.

Table 3. Comparison of fire resistance ratings obtained from numerical analyses with different parameters (governing values in bold)

Parameter	Fire Resistance According to Thermal Insulation Criterion (min)			
	For Lower-Bound Parameter Value		For Upper-Bound Parameter Value	
	Based on Max. Temp.[a]	Based on Ave. Temp.[b]	Based on Max. Temp.[a]	Based on Ave. Temp.[b]
Convective heat transfer coefficient for fire-exposed decking, $h_{c,deck}$	**135**	141	**120**	130
Convective heat transfer coefficient for unexposed top surface, $h_{c,unexp}$	**132**	139	**122**	128
Emissivity of decking, $\varepsilon_{s,deck}$	**155**	158	**117**	124
Emissivity of concrete, $\varepsilon_{s,top}$	**123**	135	**125**	136
View factor of web, Φ_{web}	**124**	137	**123**	136
View factor of upper flange, Φ_{up}	**155**	157	**122**	131
Model for thermal conductivity	**128**	136	**105**	110
Moisture content (for NWC[c])	87	**85**	**122**	131
Moisture content (for LWC[c])	**96**	98	**138**	153
Height of concrete topping, h_1	**55**	60	**247**	249
Height of rib, h_2	**121**	124	**128**	136
Width at top of rib, l_1	**128**	130	**121**	130
Width of lower flange, l_2	**122**	127	**128**	135
Width of upper flange, l_3	**139**	143	**117**	123

[a] Maximum temperature rise of ΔT = 180 °C at unexposed top surface of slab

[b] Average temperature rise of ΔT = 140 °C at unexposed top surface of slab

[c] NWC: normal weight concrete; LWC: lightweight concrete

6 Conclusions

This paper presented a detailed modeling approach for heat transfer analysis in composite slabs. The heat transfer in composite slabs was analyzed using a detailed model composed of solid elements for the concrete slab and shell elements for the steel decking. The model was validated against experimental results available in the literature. The influences of boundary conditions, thermal properties of concrete, and slab geometry on the temperature distribution within slabs were investigated. The following conclusions can be drawn from the results of this study:

(1) The fire resistance of composite slabs according to the thermal insulation criterion was generally governed by the maximum temperature rather than the average temperature at the unexposed surface. The factors that most strongly influenced the fire resistance of composite slabs were the thickness of the upper continuous portion of the slab, the emissivity of the steel decking, the view factor of the upper flange, and the moisture content of the concrete slab.

(2) The convective heat transfer coefficient had little effect on the temperature distribution of composite slabs, but the emissivity of the steel decking had a significant influence. This is

because the heat transfer from the atmosphere to the slab was dominated by radiation with a dependence on T^4. The view factor used for the steel decking significantly affected the temperature of decking but had a limited effect on temperatures within the concrete slab, which is governed by the thermal properties of concrete. The thermal boundary conditions on the unexposed surface had a negligible influence on the temperature distribution in composite slabs.

(3) The thermal conductivity of concrete had a larger influence on the temperatures at the unexposed surface than on those at the fire-exposed surface, which is governed by the thermal boundary conditions. The ASCE models of concrete conductivity are similar to the upper limit in EC4, which is recommended for the numerical analysis.

(4) The specific heat had less influence on the temperature than did the thermal conductivity. A constant specific heat value of 1000 J/(kg·K) can be used for simple analytical calculations. The moisture content of the concrete had a significant influence on the temperature distribution as expected, due to the thermal energy dissipation during water evaporation. Time histories of temperature in the concrete showed obvious plateaus at about 100 °C as the moisture content increased. An increment of 1 % in moisture content led to an increase in the fire resistance of about 5 minutes.

(5) The height of the upper continuous portion of the slab was found to be the primary geometrical factor influencing heat transfer through the slab, particularly for the thin portion of the slab. Heat transfer through the thick portion of the slab was also significantly affected by the height of the rib, and the width at the top of the rib. These two parameters significantly affected the angle of the web, through which the heat transfer had a great influence on the temperature distribution in the rib. Increasing these two parameters increased the mass in the rib, leading to reduced temperatures in the slab above the rib.

Disclaimer

Certain commercial entities, equipment, products, or materials are identified in this document in order to describe a procedure or concept adequately. Such identification is not intended to imply recommendation, endorsement, or implication that the entities, products, materials, or equipment are necessarily the best available for the purpose. The policy of the National Institute of Standards and Technology is to include statements of uncertainty with all NIST measurements. In this document, however, measurements of authors outside of NIST are presented, for which uncertainties were not reported and are unknown.

References

ASCE (1992). Structural Fire Protection. ASCE Manual and Reports on Engineering Practice No. 78. ASCE Committee on Fire Protection, New York.

Bailey C.G., White D.S. and Moore D.B. (2000). The tensile membrane action of unrestrained composite slabs simulated under fire conditions. Engineering Structures, 22: 1583-1595.

Bednar J., Wald F., Vodicka J. and Kohoutkova A. (2013). Experiments on membrane action of composite floors with steel fibre reinforced concrete slab exposed to fire. Fire Safety Journal, 59: 111-121.

Both K., Stark J.W.B. and Twilt L. (1992). Thermal shielding near intermediate support of continuous span composite slabs. Proceedings of 11th International Specialty Conference on Cold-formed Steel Structures, USA, 309-321.

Both C. (1998). The fire resistance of composite steel-concrete slabs. Ph.D. dissertation, Delft University of Technology, Delft, Netherlands.

EN 1994-1-2. (2005). Eurocode 4 Design of composite steel and concrete structures: Part 1.2: General rules, Structural fire design, European Committee for Standardization (CEN), Brussels.

EN 1991-1-2. (2009). Eurocode 1 Actions on structures: Part 1.2: General actions, Actions on structures exposed to fire, European Committee for Standardization (CEN), Brussels.

Guo S. (2012). Experimental and numerical study on restrained composite slab during heating and cooling. Journal of Constructional Steel Research, 69: 95-105.

Guo S. and Bailey C.G. (2011). Experimental behaviour of composite slabs during the heating and cooling fire stages. Engineering Structures, 33:563-571

Hamerlinck R., Twilt L. and Stark J. (1990). A numerical model for fire-exposed composite steel/concrete slabs. Proceedings of tenth International Specialty Conference on Cold-formed Steel Structures, USA, 115-130.

International Organization for Standardization (ISO). (2014.) Fire-resistance tests – Elements of building construction, ISO 834-11, Geneva, Switzerland.

Jiang J., Main J.A., Sadek F. and Weigand J. (2017). Numerical modeling and analysis of heat transfer in composite slabs with profiled steel decking. NIST Technical Note 1958, National Institute of Standards and Technology, Gaithersburg, MD.

Kirby B.R. (1997). British steel technical European fire test programme design, construction and results. Fire, static and dynamic tests of building structures. London.

Kodur V. (2014). Properties of concrete at elevated temperatures. ISRN Civil Engineering, 1-15.

Lamont S., Usmani A.S. and Drysdale D.D. (2001). Heat transfer analysis of the composite slab in the Cardington frame fire tests. Fire Safety Journal, 36:815-839.

Lamont S., Usmani A.S. and Gillie M. (2004). Behaviour of a small composite steel frame structure in a "long-cool" and a "short-hot" fire. Fire Safety Journal, 39:327-357.

Li G.Q. and Wang P.J. (2013). Advanced analysis and design for fire safety of steel structures. Zhejiang University Press, Hangzhou and Springer-Verlag Berlin Heidelberg.

Lienhard J.H. A Heat Transfer Textbook. Phlogiston Press, Cambridge, MA, 2011.

Lim L.C.S. (2003). Membrane action in fire exposed concrete floor systems. PhD Dissertation. University of Canterbury, Christchurch, New Zealand.

Lim L.C.S., Buchanan A., Moss P. and Franssen J.M. (2004). Numerical modelling of two-way reinforced concrete slabs in fire. Engineering Structures, 26:1081-91.

Livermore Software Technology Corporation (LSTC). (2014). LS-DYNA Keyword User's Manual, R7.1, LSTC, Livermore, California.

Main J.A. and Sadek F. (2012). Robustness of steel gravity frame systems with single-plate shear connections. Technical Note 1749, NIST, USA.

Nag P.K. (2008). Heat and Mass Transfer. Tata McGraw-Hill Publishing, New Delhi.

Pantousa D. and Mistakidis E. (2013). Advanced modelling of composite slabs with thin-walled steel sheeting submitted to fire. Fire Technology, 49: 293-327.

Phan, L.T., McAllister, T.P., Gross, J.L., and Hurley, M.J. (2010). Best Practice Guidelines for Structural Fire Resistance Design of Concrete and Steel Buildings. NIST Technical Note 1681, National Institute of Standards and Technology, Gaithersburg, MD.

Wellman E.I., Varma A.H., Fike R. and Kodur V. (2011). Experimental evaluation of thin composite floor assemblies under fire loading. Journal of Structural Engineering, 137(9): 1002-1016.

Zhao B., Roosefid M., Breunese A. et al. (2011). Connections of steel and composite structures under natural fire conditions (COSSFIRE). Technical Report ECSC.